

Development of Selective, Potent RabGGTase Inhibitors

E. Anouk Stigter,^{†,§,⊥} Zhong Guo,^{‡,⊥} Robin S. Bon,^{†,⊥} Yao-Wen Wu,[‡] Axel Choidas,^{||} Alexander Wolf,^{||} Sascha Menninger,[‡] Herbert Waldmann,^{†,§} Wulf Blankenfeldt,^{*,‡} and Roger S. Goody^{*,‡}

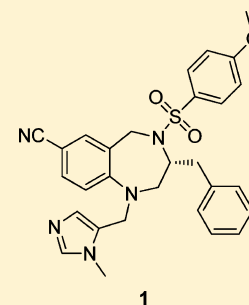
[†]Department of Chemical Biology and [‡]Department of Physical Biochemistry, Max Planck Institute of Molecular Physiology, Otto-Hahn-Strasse 11, 44227 Dortmund, Germany

[§]Fakultät Chemie, Fachbereich Chemische Biologie, Technische Universität Dortmund, Otto-Hahn-Strasse 6, 44227 Dortmund, Germany

^{||}Lead Discovery Center GmbH, Otto-Hahn-Strasse 15, 44227 Dortmund, Germany

S Supporting Information

ABSTRACT: Members of the Ras superfamily of small GTPases are frequently mutated in cancer. Therefore, inhibitors have been developed to address the activity of these GTPases by inhibiting their prenylating enzymes FTase, GGTase I, and RabGGTase. In contrast to FTase and GGTase I, only a handful of RabGGTase inhibitors have been developed. The most active RabGGTase inhibitor known until recently was an FTase inhibitor which hit RabGGTase as an off-target. We recently reported our efforts to tune the selectivity of these inhibitors toward RabGGTase. Here we describe an extended set of selective inhibitors. The requirements for selective RabGGTase inhibitors are described in detail, guided by multiple crystal structures. In order to relate in vitro and cellular activity, a high-throughput assay system to detect the attachment of [³H]geranylgeranyl groups to Rab was used. Selective RabGGTase inhibition allows the establishment of novel drug discovery programs aimed at the development of anticancer therapeutics.



■ INTRODUCTION

Prenylation is one of the crucial post-translational modifications that allow certain proteins to function properly after their synthesis in the cytosol.^{1–3} The largest protein family that undergoes prenylation is the Ras superfamily of small GTPases, in particular the Ras, Rho, Cdc42, Rac, Rap, and Rab proteins. Most members of this family need to undergo post-translational prenylation for their biological role.⁴

Different groups of the Ras superfamily are involved in diverse processes. Rab GTPases, the largest subfamily with more than 60 human members in humans, are key regulators of intracellular membrane trafficking processes.^{5,6} Covalent attachment of prenyl moieties to their C-terminal cysteines is crucial for membrane localization and hence function of these small GTPases. Ras and Rho proteins are farnesylated and geranylgeranylated at a C-terminal CAAX peptide sequence (C = cysteine, A = aliphatic amino acid, X = any residue) by the enzymes farnesyltransferase (FTase) and geranylgeranyltransferase I (GGTase I), respectively.^{7,8} In contrast, Rab GTPases are mono- or digeranylgeranylated at one or two C-terminal cysteines. Rab prenylation is mediated by Rab geranylgeranyltransferase (RabGGTase), which catalyzes two sequential geranylgeranylations for most Rabs. Because Rab GTPases do not contain a specific recognition sequence for prenylation, they are recruited by the Rab escort protein (REP); REP is responsible for recognizing Rab GTPases, presenting them to RabGGTase and delivering prenylated Rab GTPases to their target membranes.²

Ras proteins are often mutated in cancer cells, and since prenylation is essential for the function of these oncogenic

proteins, FTase and GGTase I have become popular drug targets.^{9,10} FTase and GGTase I inhibitors showed promising results in cancer cell lines and mouse models but were not as successful in clinical trials as expected.¹¹ Since some FTase inhibitors were even active in Ras-independent tumor cells,¹² it has been suggested that FTase inhibition is not their only disease modifying mode of action and that they might target additional proteins. Indeed, Lackner et al. found that some imidazole substituted tetrahydrobenzodiazepines (THBs), such as BMS3 (**1**; see Figure 1) developed by Bristol-Myers Squibb

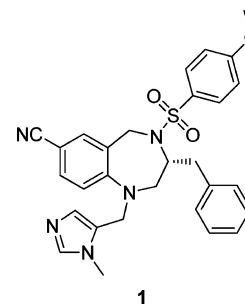


Figure 1. Dual FTase/RabGGTase inhibitor **1** (BMS3).

as FTase inhibitors, also inhibited RabGGTase. In addition, they found several genes associated with RabGTPases as strong inducers of apoptosis by using an RNAi knockdown screen in

Received: May 4, 2012

Published: September 10, 2012

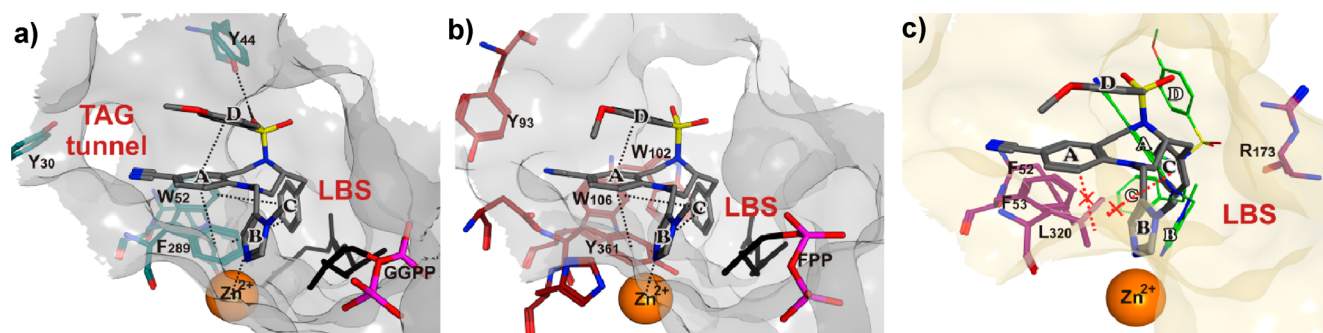
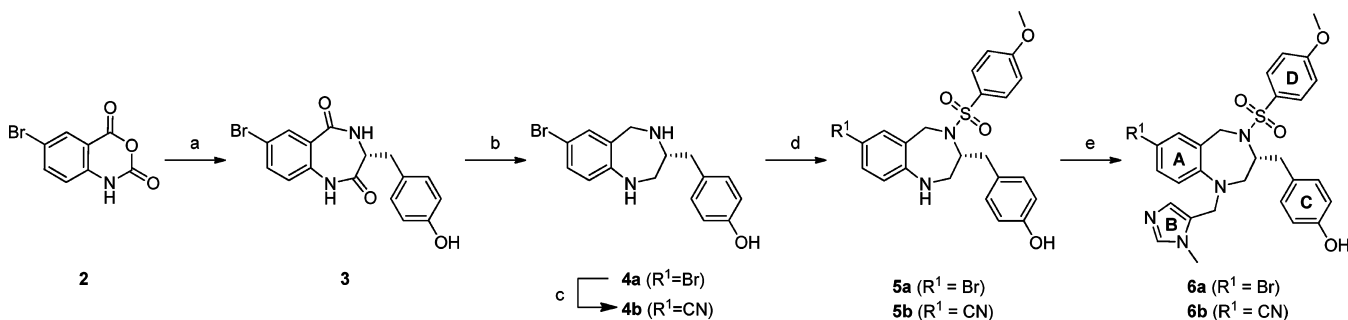


Figure 2. Comparison of active sites of RabGGTase, FTase, and GGTase I. (a) Surface representation of the active site of 1–RabGGTase–GGPP (PDB access code 3PZ2). The black dashed lines indicate ligand–protein interactions. Ring A (THB core) π -stacks with Phe289. Ring B (imidazole) binds to the zinc ion. Ring C (3-benzyl) T-stacks with Trp52 and Phe289. The sulfonyl interacts with Tyr44, and its corresponding ring D π -stacks internally with ring A. (b) Surface representation of the active site of 1–FTase–FPP (PDB access code 3PZ4). The black dashed lines indicate ligand–protein interactions. Ring A (THB core) π -stacks with Tyr361. Ring B (imidazole) binds to the zinc ion. Ring C (3-benzyl) T-stacks with Trp102, Trp106, and Tyr 289. Ring D π -stacks internally with ring A and is mainly solvent exposed. (c) Superposed **1** (gray sticks) and docked **1** (green wire) in the active site of GGTase I (PDB access code 1S64). GGTase I has less aromatic residues in the binding site; therefore, stabilizing π - and T-stacking interactions with rings A and C are not realized (red dashed lines). Docking studies show no consensus for **1** binding (best solution is shown in green sticks). The lack of interaction partners for **1** seems to ensure selectivity over GGTase I toward RabGGTase and FTase. Crystal structures are shown in gray, and docked structures are shown in yellow.

Scheme 1. Synthesis of General Building Blocks for THB-Based Libraries^{21a}



^aReagents and conditions: (a) D-tyrosine methyl ester hydrochloride, DMAP, pyridine, reflux, 3 days, 68%; (b) BH_3 in THF, reflux, 16 h, 67% (or 60% over two steps when **3** was not purified); (c) CuCN , DMF, 210 °C (microwave), 70%; (d) 4-methoxybenzenesulfonyl chloride, pyridine, 0 °C to rt, 16 h, 71% ($R = \text{Br}$) or 61% ($R = \text{CN}$); (e) 1-methylimidazole-5-carboxaldehyde, TFA, TFAA, triethylsilane, rt, 16 h, 80% ($R = \text{Br}$) or 83% ($R = \text{CN}$).

C. elegans. These include Rab5, Rab7, and the HOPS complex that interacts with Rab7. In addition RNAi against the RabGGTase- α and RabGGTase- β subunits was effective in inducing apoptosis. In contrast, RNAi against FTase- β or GGTase I- β had no effect on induction of apoptosis in *C. elegans*.¹³

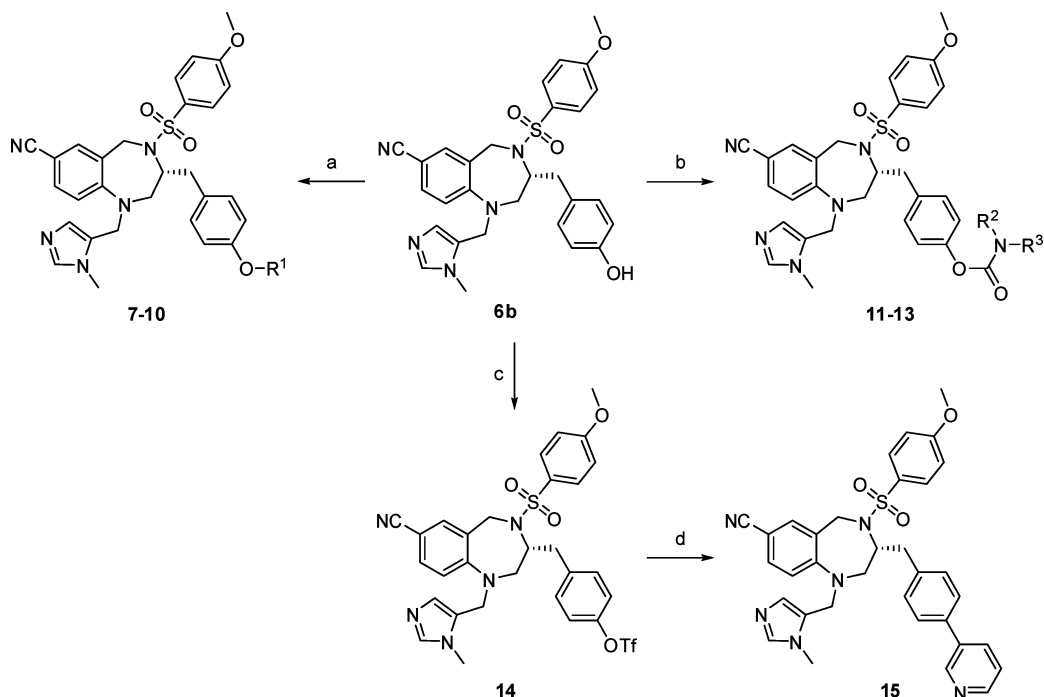
Rab GTPases and their interacting proteins are involved in cancer, genetic diseases, and pathogen uptake mechanisms.^{6,14} However, only a few RabGGTase inhibitors have been developed.^{15–18} Phosphonocarboxylate inhibitors led to the development of a low micromolar, specific RabGGTase inhibitor, inhibiting only the first prenylation step.^{19,20} Recently, we reported a potent highly selective RabGGTase inhibitor, which inhibits cellular Rab prenylation and proliferation of several cancer cell lines without displaying general cytotoxicity to human peripheral blood cells (PMBCs).²¹

Here we describe in detail the requirements for selective RabGGTase inhibitors, using the tetrahydrobenzodiazepine (THB) as a guiding scaffold. While previous studies gave first insights into the requirements for selectivity, we have now designed selective inhibitors based on the exploration of different substituents around the THB core and crystallization studies with both FTase and RabGGTase. In order to relate in vitro and cellular activity, a high-throughput assay system, using scintillation proximity

beads to detect the transfer of [³H]geranylgeranyl groups from [³H]GGPP to Rab, was established.

RESULTS AND DISCUSSION

Comparison of the Active Sites: FTase, RabGGTase, and GGTase I. The THB scaffold already ensures selectivity for RabGGTase and FTase with respect to GGTase I.²¹ Comparison of the active sites for the 1–RabGGTase–GGPP complex and the 1–FTase–FPP complex from our previously published work with the active site of GGTase I allowed us to delineate initial insights into activity and selectivity requirements.²¹ An overlay of the active site in 1–RabGGTase with the active site of GGTase I shows that the THB core cannot form similarly favorable van der Waals interactions because of the absence of aromatic residues in the GGTase I binding site. In contrast, the presence of multiple aromatic residues in both the FTase and RabGGTase active sites allows efficient binding of THBs with similar potency (Figure 2). These observations are supported by the solutions obtained by virtual screening carried out for FTase, GGTase I, and RabGGTase. In contrast to the solutions obtained for **1** in FTase and RabGGTase, no binding consensus was found for **1** in GGTase I (for details see the Supporting Information). Small molecules comprising

Scheme 2. Introduction of Substituents To Address the LBS^a

^aReagents and conditions: (a) alkyl bromide, NaH, DMF, rt, 85–94%; (b) carbamoyl chloride or isocyanate (for R² = H), Et₃N, DCM, rt, 72–98%; (c) TfN(Ph)Tf, Et₃N, DCM, 0 °C to rt, 94%; (d) pyridine-3-boronic acid, Pd(PPh₃)₄, K₂CO₃, DME/H₂O, 80 °C, 16 h, 94%.

π -stacking and T-stacking elements close to the zinc binding group thus appear to distinguish GGTase I from RabGGTase and FTase.

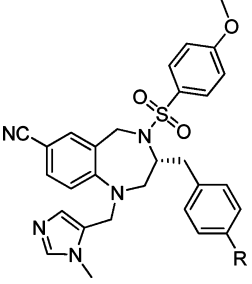
To achieve further selectivity, there are two major differences between RabGGTase and FTase that can be exploited. One unique feature of RabGGTase is a tunnel adjacent to the GGPP binding site, the so-called TAG tunnel, identified during the evaluation of peptide-based selective RabGGTase inhibitors.¹⁷ The second opportunity to create selective inhibitors is presented by the lipid binding site (LBS). Extensions into or near the LBS were expected to be accommodated in RabGGTase while generating a clash with Trp102 of FTase, an aromatic residue in FTase that is the main determinant of FPP over GGPP selectivity (Figure 2).²¹ However, inhibitors extended to either one of these sites, unexpectedly, were not sufficient to obtain high selectivity. To obtain a deeper insight into the requirements for selectivity toward RabGGTase with respect to FTase at the molecular level, we developed a larger subset of THBs and, together with previously reported THBs,²¹ subjected them to a range of prenylation assays and crystallization experiments.

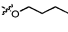
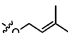
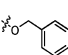
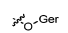
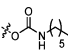
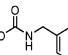
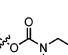

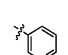
Synthesis of the General Building Block. The necessary building blocks for the THB series were synthesized according to previously published procedures (Scheme 1).²¹ In short, condensation of 5-bromoisatoic anhydride **2** with D-tyrosine-methyl ester led to 7-bromo-1,4-benzodiazepine-2,5-dione **3**, which was reduced to the corresponding tetrahydrobenzodiazepine (THB) **4a** using borane in THF. Subsequent copper catalyzed cyanation led to the formation of **4b**, the building block for the first generation of inhibitors, meant to target the LBS. Compound **4a**, containing the 7-bromo substituent, served as a precursor for the later generations of THBs, meant to target the TAG tunnel. Introduction of the sulfonamide moiety via selective N-sulfonylation by use of a weak base such as pyridine led to **5a** and **5b**. The imidazolylmethyl group was subsequently

introduced by reductive amination to obtain building blocks **6a** and **6b**.

Synthesis and Analysis of THBs Targeting the LBS. To study the influence of different substitutions of **6b** directed toward the GGPP binding site on inhibitory activity and selectivity, the phenol group of **6b** was derivatized using a range of reactions (Scheme 2). Alkylation was achieved in high yields by addition of an alkyl, allyl, or benzyl bromide with sodium hydride as a base (Table 1). Aminoacylation was performed by addition of either an isocyanate or a carbamoyl chloride in the presence of base, leading to the corresponding products in excellent yields. Building block **14** was obtained in high yield using the triflating reagent *N*-phenyl-bis(trifluoromethanesulfonimide), whereas standard conditions using triflic anhydride gave **14** in only 55%. The triflate was subjected to coupling with pyridine-3-boronic acid under standard Suzuki coupling conditions. This variety of modifications resulted in the first generation of inhibitors based on **1** and emphasizes the phenolic hydroxyl group as a versatile handle for modification.

Because these extensions approach the LBS, we reasoned that the obtained inhibitors could result in different inhibition modes with respect to GGPP. Therefore, we decided to analyze the compounds using a radiometric [³H]GGPP assay that was expected to resemble the native situation more closely than the fluorometric NBD-FPP assay used previously.²¹ The radiometric assay allows a double geranylgeranylation reaction, and [³H]GGPP obviously has a *K_d* equal to that of GGPP. The latter feature could be important to predict cellular activity for inhibitors that are competitive with GGPP or for inhibitors that interact with the isoprenoid group. In order to screen a large set of substances, the radiometric assay was adapted to a high-throughput format using scintillation proximity beads (see Experimental Section for details).

Table 1. Synthesis and Biological Evaluation of RabGGTase Inhibitors Approaching the Lipid Binding Site^a


Entry	Cmpd	R	Yield	FTase	<i>In vitro</i> IC50 [nM]			IF ^{RA}
					RabGGTase ^{RA}	RabGGTase ^{FL}	GGTase I	
1	1	H	-	6±3	6.4±4.8	724±321	>99,500	1.00
2	6b	OH	-	5.2±0.2	<4 ^{\$}	1,011±465	>99,500	1.39
3	7		92%	10±7	156±49	162±10	>99,500	0.1
4	8		94%	15±8	63±24	39±10	>99,500	0.3
5	9		85%	99.3±59	181±14	441 [#]	>99,500	0.59
6	10		94%	1,012±688	23.5±4.5	2,072 [#]	>99,500	45.93
7	11		98%	9.2±4.2	15.5±1.5	243±20	>99,500	0.63
8	12		96%	<5 ^{\$}	6±4	72±2	>99,500	0.89
9	13		72%	<5 ^{\$}	123±22	38±7	2,020±384	0.04
10	14		94%	10.5±3.9	1496±100	>9,500	>99,500	0.01
11	15		94%	4.3±2.2	11±2	353±158	3,632±15	0.42

^aFL= fluorometric assay. RA= radiometric assay. (\$) Lower detection limit. (#) single point measurement. ger = geranyl. IF = improvement factor.

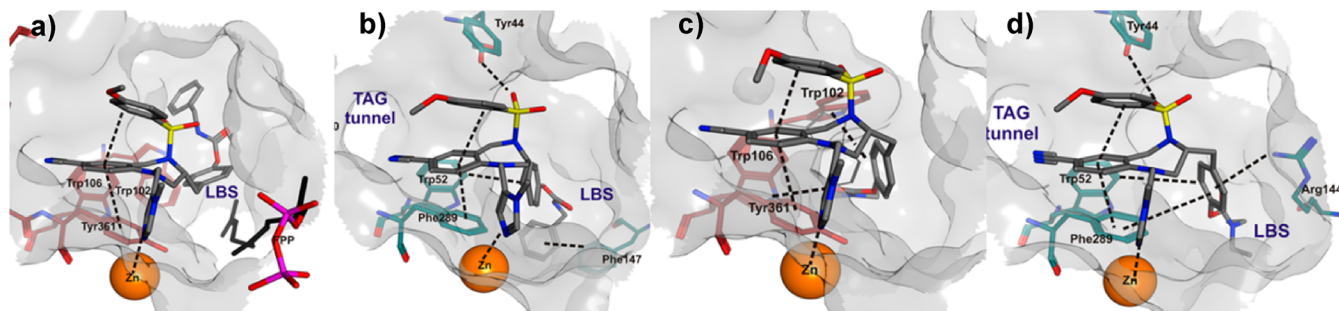
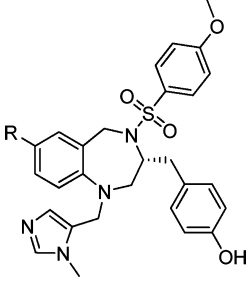
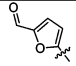
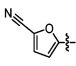
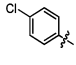
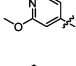
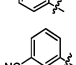
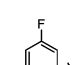
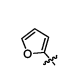
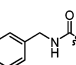
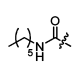
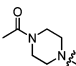
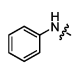
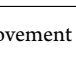


Figure 3. Cocrystal structures of **12** and **13**. (a) Surface representation of active site of the **12**–FTase–FPP complex (PDB access code 4GTQ). Similar to BMS3, the imidazole coordinates to the zinc ion. The THB interacts with Tyr361 and is further involved in internal π -stacking with the anisylsulfonyl group. The 3-benzyl moiety extends to the back, disrupting the interactions with Trp102 and Trp106. The black dashed lines indicate interactions between ligand and enzyme. (b) Surface representation of the active site of **12**–RabGGTase complex (PDB access code 4GTT). Similar to **1**, the imidazole coordinates to the zinc ion, whereas the sulfonamide forms hydrogen bonds with Tyr44. The 3-benzyl moiety interacts with Trp52 and Phe289 by edge–face hydrophobic stacking, whereas the THB moiety stacks face–face with Phe289. The conformation is further stabilized by internal π -stacking of the THB with the anisylsulfonyl group. The additional benzylcarbamate contributes with an edge–face hydrophobic stacking with Phe147. The black dashed lines indicate interactions between ligand and enzyme. (c) Surface representation of active site of **13**–FTase complex (PDB access code 4GTR). The imidazole coordinates to the zinc ion. The THB interacts with Tyr361 and is further involved in internal π -stacking with the anisylsulfonyl group. The additional diethylcarbamate functionality is adopted via a reorientation of Trp102 by 180° and forms hydrogen bonds with Trp106. The black dashed lines indicate interactions between ligand and enzyme. (d) Surface representation of the active site of **13**–RabGGTase complex (PDB access code 4GTV). Similar to **1**, the imidazole coordinates to the zinc ion, whereas the sulfonamide forms hydrogen bonds with Tyr44. The 3-benzyl moiety interacts with Trp52 and Phe289 by edge–face hydrophobic stacking, whereas the THB moiety stacks face–face with Phe289. The conformation is further stabilized by internal π -stacking of the THB with the anisylsulfonyl group. The additional diethylcarbamate contributes with cation– π -stacking with Arg144. The black dashed lines indicate interactions between ligand and enzyme.

Table 2. Synthesis and Screening of THB-Based Inhibitor Meant To Target the TAG Tunnel^a


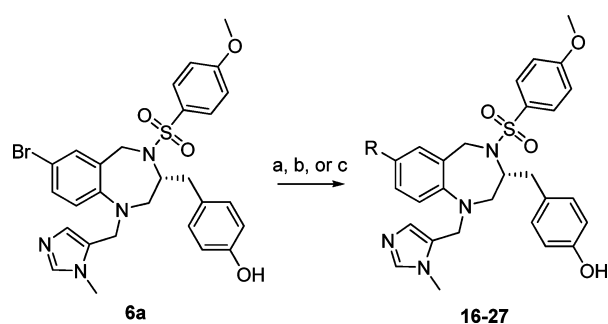
entry	cmpd	R1	Yield	<i>In vitro</i> IC ₅₀ [nM]			IF
				RabGGTase	FTase	GGTase 1	
1	1	CN	-	6.4±4.8	6±3	>99,500	1.0
2	16		68%	12.8±8.8	11.4±10	>99,500	1.0
3	17		66%*	<14 [§]	26.9±20	>99,500	2.0
4	18		77%	706±246	194±78	>99,500	0.29
5	19		40%	5.5±1.5	18.6±0.6	>99,500	3.6
6	20		68%	<4 [§]	13.6±8.6	>99,500	3.6
7	21		52%	22.5±7.5	34.4±21.2	>99,500	1.6
8	22		82%	185±8	172±117	>99,500	1.0
9	23		61%	55±10	81.7±70.3	>99,500	1.6
10	24		16%	19±2	7±1.6	>99,500	0.4
11	25		13%	70.5±11.5	20.7±4.6	>99,500	0.3
12	26		30%	27±6	112±91	>99,500	4.4
13	27		33%	246.5±52.5	454±207	>99,500	2.0

^a(§) Lowest detection limit. IF = improvement factor. (*) Prepared from **17** in two steps: (a) NH₂OH·H₂O, Et₃N, DCM/MeOH; (b) TFAA, DCM, rt.

The assay results are summarized in Table 1. The previously reported activity in the NBD-FPP assay is also included for comparison.²¹ The IC₅₀ values measured in the radiometric assay for **1** resemble the previously reported activity determined in a [³H]GGPP filter binding assay (IC₅₀ = 21 nM).¹³ The data clearly suggest a different trend for this compound set in the [³H]GGPP and NBD-FPP assays, respectively, which in most cases results in higher IC₅₀ values compared to **1** (e.g., compounds **7**, **8**, and **13**). The difference in IC₅₀ values between the two assay systems suggests different interactions of the different lipid substrates with RabGGTase. For this generation of inhibitors only the incorporation of a benzylcarbamate or

3-pyridine resulted in compounds as active as **1** in the radiometric assay. Competition experiments with NBD-FPP indeed showed different binding modes due to additional extensions (for experimental details, see the Supporting Information). Compound **10** was found to be competitive with regard to the lipid substrate, whereas **1** was noncompetitive. Most extensions had less effect on FTase than expected based on the predicted clash with Trp102, thus still showing significant FTase inhibition. In order to find an explanation for the observed trends, crystallization studies were carried out. Inhibitors **12** and **13** could be successfully soaked into both FTase and RabGGTase (Figure 3). The cocrystal structures revealed that the binding

Scheme 3. Introduction of Substituents To Address the TAG Tunnel^a



^aReagents and conditions: (a) arylboronic acid, Pd(PPh₃)₄, K₂CO₃, DME/H₂O 2/1, 40–82%; (b) amine, Mo(CO)₆, Fu's salt, Hermann's palladacycle, DBU, THF, 160 °C (microwave), 13–16%; (c) amine, NaO-*t*-Bu, Pd₂(dba)₃, JohnPhos, THF, reflux or 100 °C (microwave), 30–33%.

mode of the THB moiety is highly conserved in the two enzymes. The π -stacking of ring A with the aromatic enzyme residues and imidazole zinc binding locks the seven-membered ring connected to the imidazole moiety in an L-shaped fashion. The orientation of the phenolic portion (ring C), either connected to a phenylcarbamate or diethylaminecarbamate, appears to be more flexible; **12** shows a conformational change in this area, while **13** adopts the same conformation as **1**.

In the complex **12**–FTase–FPP structure (Figure 3a) this conformational change, which also leads to loss of some hydrophobic interactions, is the main difference between **12** and parent compound **1**. However, this difference does not result in a decrease in potency of inhibition. In the complex **12**–RabGGTase structure (Figure 3b) an additional hydrogen bond between the sulfonyl group of the ligand and Tyr44 is formed. There also appears to be an additional hydrophobic interaction between the introduced benzylcarbamate and the lipid binding site of the enzyme. The cocrystal structure of **13**–FTase (Figure 3c) revealed that the Trp102 residue, originally contributing with an edge–face T-stacking interaction, is flipped by 180°. This opens up extra space in the hydrophobic area, allowing the extended THBs to bind. However, an

additional hydrogen bond interaction is formed between Trp106 and the diethylcarbamate group. In total, these changes result in an approximately similar IC₅₀ for FTase. In the complex **13**–RabGGTase (Figure 3d), additional interactions are realized by a cation– π interaction between Arg144 and the 3-benzyl moiety (ring C).

The crystal structure analysis shows that both the inhibitors and the FTase binding site adopt different conformations due to the extensions of the THBs, resulting in selectivity profiles similar to that of **1**. This accentuates the need for extensions in other or additional directions to obtain selective inhibitors.

Design, Synthesis, and Assaying of THBs Approaching the TAG Tunnel. Since the new insights obtained from the cocrystal structures indicated the need for different and/or additional extensions to the candidate substances, we decided to introduce additional substituents toward the RabGGTase specific TAG tunnel. Incorporation of substituted aromatic rings would most probably result in a clash with the RabGGTase surface, which would disrupt the important π -stacking with the THB moiety (ring A) and imidazole zinc binding.²¹ In order to identify additional promising candidates to the previously identified furan moiety (Table 2, entries 2 and 3), we carried out a virtual high throughput screening (VHTS) with conformational constraints. A virtual library was created using Pipeline Pilot by assembly of the THB core structure with various substituents. The compounds in the library were minimized in energy to obtain their local-minimum 3D-conformations, which were used as input for the virtual screening. The enzymes were prepared for docking by removal of the inhibitors and prenyl pyrophosphates followed by the addition of hydrogens using the Protonate3D function in MOE. All members in the virtual library were docked in both RabGGTase and FTase using GOLD. In RabGGTase, the conformation of the THB was fixed between Phe289 and the zinc ion in order to mimic the π -stacking and imidazole zinc interaction, which seems essential for activity (see Supporting Information). Compounds that scored high for RabGGTase and low for FTase were expected to represent selective RabGGTase inhibitors that correctly approach the TAG tunnel. Several groups in addition to the furanaldehyde (**16**) and furannitrile (**17**) could be identified. Heteroaromatic groups such as pyridine point toward the TAG tunnel without distorting the general binding character.

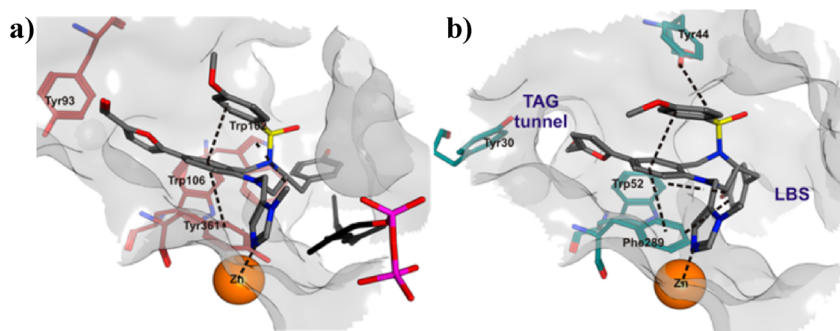
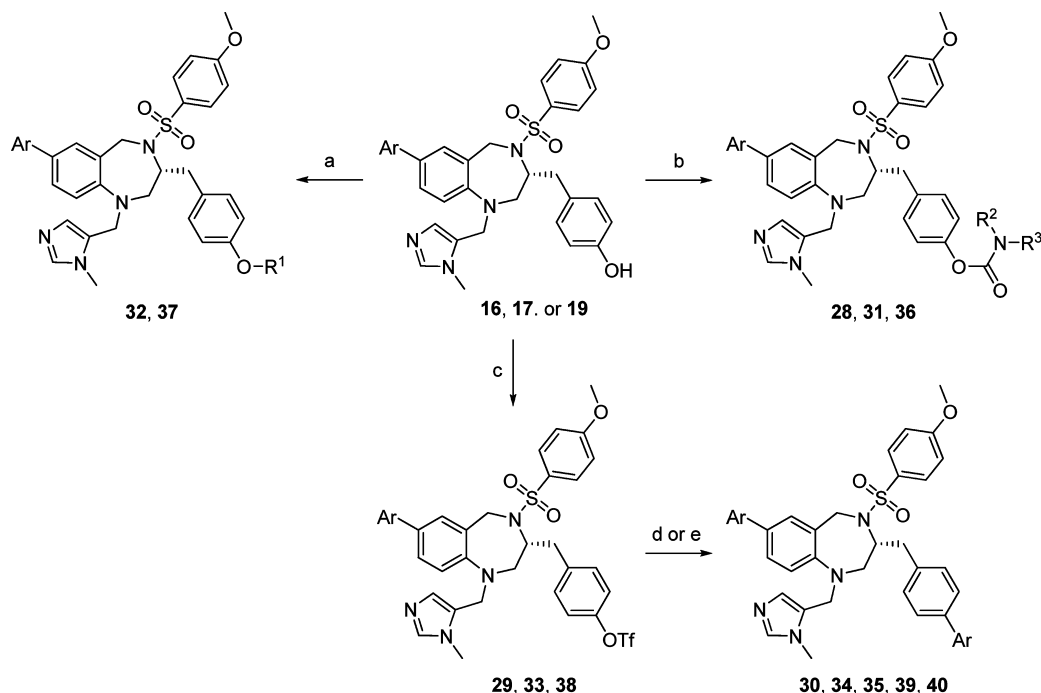


Figure 4. Cocrystal structures of **16** in FTase and RabGGTase. (a) Surface representation of active site of **16**–FTase–FPP complex (PDB access code 4GTP). The imidazole coordinates to the zinc ion. The THB interacts with Tyr361 and is further involved in internal π -stacking with the anisylsulfonyl group. The additional furanal barely fits in the FTase pockets and induces a conformational change of the 3-benzyl moiety, disrupting the favorable hydrophobic interactions with Trp106. The black dashed lines indicate interactions between ligand and enzyme. (b) Surface representation of the active site of **16**–RabGGTase complex (PDB access code 4GTS). Similar to **1**, the imidazole coordinates to the zinc ion, whereas the sulfonamide forms hydrogen bonds with Tyr44. The 3-benzyl moiety interacts with Trp52 and Phe289 by edge–face hydrophobic stacking, whereas the THB moiety stacks face–face with Phe289. The conformation is further stabilized by internal π -stacking of the THB with the anisylsulfonyl group. The additional furanal occupies the entrance of the TAG tunnel, but the expected hydrogen bond interaction between the aldehyde and Tyr30 cannot be observed. The black dashed lines indicate interactions between ligand and enzyme.

Scheme 4. Synthesis of THBs Targeting Both the TAG Tunnel and LBS^a

^aReagents and conditions: (a) alkyl bromide, NaH, DMF, rt, 69–81%; (b) benzyl isocyanate, Et₃N, DCM, rt, 71–86%; (c) TfN(Ph)Tf, Et₃N, DCM, 0 °C to rt, 86–99%; (d) arylboronic acid, Pd(PPh₃)₄, K₂CO₃, DME/H₂O, 80 °C, 68–84%; (e) aniline, NaO-*t*-Bu, Pd₂(dba)₃, JohnPhos, toluene, reflux, 43–75%.

Other suggestions from VHTS were flexible groups such as *N*-acetylpiperazine, which could adjust toward the TAG tunnel. This group would have the additional advantage of increasing the solubility of the compounds.

The suggestions from VHTS could be verified by synthesis using transition metal based cross-coupling procedures on building block **6a** (Scheme 3). The Suzuki coupling with heteroaromatic rings resulted in low to moderate yields (e.g., **19**, 40%), most probably related to the instability of the boronic acid counterpart. Aminocarbonylation using Herrmann's palladacycle, air stable Fu's salt [(*t*-Bu)₃PH]BF₄, and molybdenum hexacarbonyl under microwave irradiation afforded **24** and **25**. Buchwald–Hartwig couplings of **6a** and *N*-acetylpiperazine or aniline gave THBs **26** and **27**. The new compound set was screened against the three prenyltransferases (Table 2).

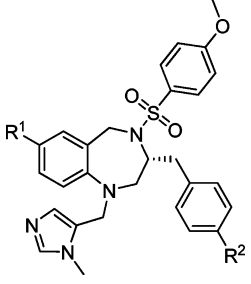
Table 2 reveals that the introduction of five-membered rings as well as the introduction of pyridine derivatives and amine linkers led to enhanced selectivity for RabGGTase (1- to 4.4-fold enhancement). The introduction of larger groups such as amides (entries 8 and 9) results in a slight preference for FTase. Interestingly, the previously reported para-chloro-substituted THB (**18**) still showed some remaining activity in the radioactive assay, although it is 100-fold less potent than **1**. The binding mode of this second generation of inhibitors, determined for **18** and **20**, was, as expected, noncompetitive with respect to NBD-FPP (see Supporting Information). However, also for this second generation of inhibitors, complete selectivity was not reached for RabGGTase over FTase. One plausible explanation could be that the additional groups could orient toward the exit groove of FTase, thereby preventing a clash with the surface. In order to test this hypothesis, we subjected the inhibitors to crystallization studies in both FTase and RabGGTase. We successfully solved the

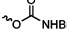
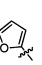
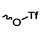
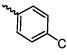
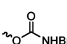
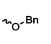
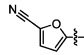
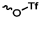
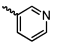
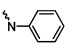
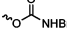
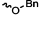
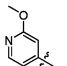
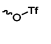
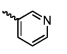
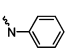
crystal structures of **16**–FTase–FPP and **16**–RabGGTase (Figure 4).

The cocrystal structure of **16**–FTase–FPP revealed that the addition of the furanal at R¹ results in a compressed binding mode. The furanal moiety barely fits into the small hydrophobic space and, as expected, orients toward the exit groove of the active site, which seems to result in a conformational change at the other end of the ligand. In order to keep the favorable conformation for π -stacking and zinc binding, the phenolic portion of the molecule turns by 180°, a similar phenomenon as seen for ligand **12**. This causes the loss of favorable hydrophobic interactions with the binding site Trp residues (Figure 3a). In complex **16**–RabGGTase, the furanal moiety orients toward the TAG tunnel. Further, the structure closely resembles the **1**–RabGGTase complex, showing the same binding mode and conformation (Figure 3b). The inhibitor does not occupy the lipid binding site, which was expected from both VHTS and competition experiments.

The crystal structures of the complexes with compounds targeting either the LBS or the TAG tunnel complement the *in vitro* data. Obviously, extension of the THB in only one direction is not sufficient for selectivity. The predicted clashes with the binding site of FTase were circumvented via reorientation of Trp102 in the enzyme or via adoptive behavior of the ligand.

Design, Synthesis, and Assaying of Inhibitors Approaching Both the LBS and TAG Tunnels. Interestingly, in FTase, the introduction of the furanal moiety induces a conformational change of the 3-benzyl moiety, which approaches the surface region of FTase composed of residues Ala151, Arg202, and Trp102. This could also explain the selectivity of previously reported **28**, bearing extensions toward both sides.²¹ This new binding pose thus shows an increased likelihood to obtain selective RabGGTase inhibitors by combining

Table 3. Synthesis and Evaluation of Inhibitors Targeting Both the RabGGTase TAG Tunnel and the LBS^a


entry	compd	R ¹	R ²	Yield ^b	<i>In vitro</i> IC ₅₀ [nM]			
					RabGGTase	FTase	GGTase I	IF
1	1	CN	H	-	6.4±4.8	6±3	>99,500	1.0
2	16		OH	-	12.8±8.8	11.4±10	>99,500	0.95
3	28			82% ^a	1,547±101	>9,700	>99,500	Nc
4	29			86% ^c	4,292±1,327	>9,700	>99,500	Nc
5	30			84% ^c	2,240±1,235	>9,700	>99,500	Nc
6	17		OH	-	<14 ^b	26.9±20	>99,500	2.0
7	31			71% ^a	260±18	>9,700	>99,500	Nc
8	32			69% ^b	577±282	>9,700	>99,500	Nc
9	33			99% ^c	nd	nd	nd	Nd
10	34			68% ^c	37±21	109.9±41.1	>99,500	3.2
11	35			43% ^d	1,056±41	1,212±261	>99,500	1.2
12	19		OH	-	5.5±1.5	18.6±0.6	>99,500	3.6
13	36			86% ^a	55±11	321±291	>99,500	6.2
14	37			81% ^b	5,245±1,129	2,556±545	>99,500	0.5
15	38			90% ^c	nd	nd	nd	nc
16	39			84% ^c	121.3±3.3	79±13.3	>99,500	0.7
17	40			75% ^d	5,719±1,765	2,432±2,182	>99,500	0.5

^a(§) Method used. (§) Lower detection limit. nc = not calculated. nd = not determined. IF = improvement factor.

substituents that approach both the TAG tunnel and the LBS. In order to obtain a representative, larger set of selective substances, we combined the most active groups of generations 1 and 2 to obtain additional active and selective RabGGTase inhibitors. In addition, we carried out an additional virtual screening with GGPP in the binding site of RabGGTase to identify substituents that were predicted to be compatible with GGPP (see Supporting Information). These GGPP-compatible groups would give the opportunity to compare the difference between competitive and uncompetitive inhibitors.

To obtain a set of inhibitors approaching both the LBS and the TAG tunnel, we followed a similar strategy as described above. First R¹ was decorated by means of transition-metal-catalyzed coupling reactions, after which R² was substituted using various strategies (Scheme 4). The results for this generation are listed in Table 3. Introduction of substituents pointing toward

both the TAG tunnel and the LBS resulted in a set of selective RabGGTase inhibitors (**28**, **29**, **30**, **31**, **32**). In contrast to the data previously reported using the fluorometric NBD-FPP assay²¹ all combinations resulted in a 10- to 1000-fold decrease in inhibition of RabGGTase, which would suggest competitive binding modes for most compounds with respect to GGPP. Competition experiments with **28** and NBD-FPP showed, however, that **28** was noncompetitive with respect to NBD-FPP. The GGPP-compatible design principle, represented by compounds **34**, **35**, **39**, and **40**, showed mixed success. The THBs decorated with aniline (**35**, **40**), which were predicted to give stabilizing hydrophobic interactions with the two terminal isoprene units of GGPP, were practically inactive for both enzymes. In contrast, the THBs extended with 3-pyridine (**34**, **39**) that should give similar stabilizing hydrophobic interactions yielded the most active inhibitors targeting the LBS.

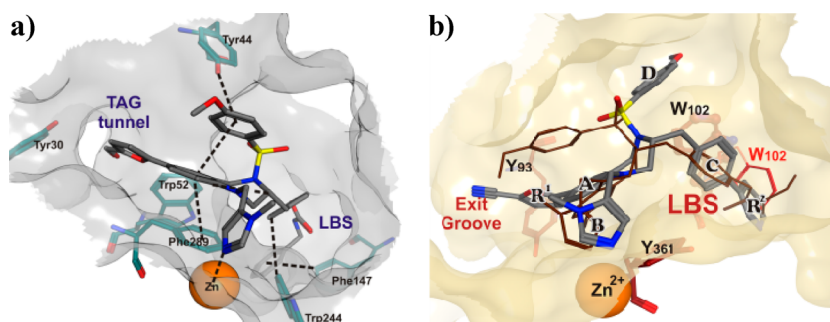


Figure 5. (a) Surface representation of the active site of the **28**–RabGGTase complex (PDB access code 3PZ3). Similar to **1**, the imidazole coordinates to the zinc ion, whereas the sulfonamide forms hydrogen bonds with Tyr44. The 3-benzyl moiety interacts with Trp52 and Phe289 by edge–face hydrophobic stacking, whereas the THB moiety stacks face to-face with Phe289. The conformation is further stabilized by internal π -stacking of the THB with the anisylsulfonfyl group. The additional furanal occupies the entrance of the TAG tunnel, but the expected hydrogen bond interaction between the aldehyde and Tyr30 cannot be observed. The additional benzylcarbamate contributes with an edge–face hydrophobic stacking with Phe147. The black dashed lines indicate interactions between ligand and enzyme (adapted from Bon et al.²¹). (b) Surface representation of the active site of **13**–FTase (PDB access code 4GTR) with **34** docked in the active site. The docking solution shows that R² would fit in the enlarged pocket caused by Trp102 rotation. An overlay of the original Trp102 position exemplifies the clash.

Unfortunately, this was the case for both RabGGTase and FTase. This finding suggests that the introduction of this moiety leads to a similar behavior in FTase as observed with compound **13** (Figure 3).

In order to find an explanation for the observed dual activity of compound **34**, we docked the structure to the FTase surface of **13**–FTase–FPP and compared it to the solution obtained for the docking in **1**–FTase–FPP. Indeed, the docking score observed in **13**–FTase–FPP was significantly higher than the original score in **1**–FTase–FPP (Figure 5b). This supports the hypothesis that the flexibility of Trp102 leads to more tolerance toward enlarged THBs.

Attempts to crystallize the third generation of inhibitors with FTase and RabGGTase were successful for **28** with RabGGTase, as reported previously (Figure 5a).²¹

Cellular Assays. The complete set of inhibitors was evaluated for their potential to inhibit cellular RabGGTase prenylation using a previously described method (reprenylation assay)²² and to inhibit proliferation of several cancer cell lines. The results are summarized in Table 4. It is important to note that most tested inhibitors are inactive up to 10 μ M in the PBMC assay, providing first indications that this compound class is not generally cytotoxic.

The compounds all have different selectivity profiles. Compound **14** is a selective FTase inhibitor, whereas **28** and **31** are selective RabGGTase inhibitors. The other compounds are all dual inhibitors, with different potencies for RabGGTase and FTase. It could be shown that the selective RabGGTase inhibitors (**28**, **31**) both resulted in inhibition of cancer cell proliferation. Compound **31**, a selective inhibitor of RabGGTase with a similar cellular potency against RabGGTase as **1**, inhibited proliferation of all cancer cell lines as potently as the dual inhibitor **1**. Interestingly, the selective FTase inhibitor **14** with a similar FTase potency as **1** only retained its activity against A2780 cells. These results indicate that inhibition of RabGGTase alone is sufficient to inhibit cancer cell proliferation, whereas the efficiency of inhibition of FTase seems to be more cancer cell line specific. Close inspection of the data revealed similar trends. Dual inhibitor **13**, which showed potent FTase and moderate RabGGTase activity, effectively inhibited proliferation of the HCT116 and A2780 cells but showed a clear drop in activity for HeLa cells. These data were complemented by the activity profile of dual inhibitor **12**, showing potent RabGGTase and FTase

inhibition. In this case, the inhibition of proliferation of HeLa cells was retained whereas the activity against HCT116 and A2780 slightly dropped. These data combined suggest that HCT116 and A2780 cells are more sensitive to FTase inhibition than HeLa cells.

Comparison of inhibitors **31** and **34** shows that the GGPP compatible design is not as crucial for inhibition of cellular prenylation as has been observed in the in vitro assays. One explanation could be that the GGPP concentration in the cells is different from the GGPP concentration in the radiometric assay and hence has less impact on the inhibition. The concentration of GGPP in NIH/3T3 cells has been determined at 0.145 pmol/10⁶ cells,²³ which would correspond to approximately 65 nM GGPP and is 30-fold less than that used in the in vitro assay.

Inhibitor **17**, which shows a remarkable cellular inhibition of RabGGTase and moderate in vitro inhibition of FTase, shows a significant effect on cancer cell line proliferation, giving IC₅₀ values in the range of 2–21 nM. This demonstrates the potential of low nanomolar inhibitors of RabGGTase to inhibit cancer cell proliferation.

CONCLUSION AND OUTLOOK

Diversification of the THB scaffold by an iterative cycle of synthesis, screening, and design guided by crystal structure determination led to the conversion of a dual FTase/RabGGTase inhibitor into potent, selective, not generally cytotoxic RabGGTase inhibitors. Selective inhibitor **31** (49 nM, cellular IC₅₀) inhibits cancer cell proliferation as potently as dual inhibitor **1** and shows the potential of selective RabGGTase inhibition for novel drug discovery programs aimed at the development of anticancer therapeutics.

The selectivity prerequisites for RabGGTase, FTase, and GGTase I uncovered here could be used while exploring additional scaffolds. An interesting approach that could be pursued would be a fragment-based design. Crystal structures with (low affinity) fragments could reveal additional RabGGTase specific interaction partners. In addition, it would increase the chance to identify motifs that would accommodate to the TAG tunnel.

Additional studies to confirm the therapeutic relevance of RabGGTase will give extra insight into the effect of RabGGTase inhibition and hence Rab GTPase disturbance.

Table 4. Cellular Evaluation of Selected Inhibitors (IC₅₀ in nM)

compd	RabGGTase (NBD-FPP)	RabGGTase ([³ H]GGPP)	cellular prenylation	FTase	HCT116	HeLa	A2780	A549	DUI45	PBMC
1	724 ± 321	6.4 ± 4.8	74 ± 34	6 ± 3	63 ± 8	101 ± 2	43	99 ± 18	70 ± 8	>10000
6b	1011 ± 465	4	114.9 ± 59.5	5.2 ± 0.2	172 ± 34	130 ± 6	100 ± 24	315 ± 12	162 ± 4	nd
7	162 ± 10	156 ± 49	307 ± 40	10 ± 7	264 ± 28	154 ± 4	165 ± 1	216 ± 52	241 ± 43	8686
8	39 ± 10	63 ± 24	43 ± 12	15 ± 8	112 ± 2	59 ± 2	116 ± 8	74 ± 22	90 ± 2	8028
9	441	180.5 ± 13.5	nd	99.3 ± 59	1048 ± 435	372 ± 1	265 ± 79	746 ± 96	756 ± 38	>10000
10	2072	23.5 ± 4.5	278	1012 ± 688	1434 ± 484	nd	1381 ± 280	653 ± 174	nd	>10000
11	243 ± 20	15.5 ± 1.5	77.3 ± 1.7	9.2 ± 4.2	355 ± 118	nd	233 ± 25	389 ± 42	228 ± 23	nd
12	72.2 ± 1.7	6 ± 4	81 ± 32	<5	231 ± 59	151 ± 21	130 ± 9	338 ± 82	142 ± 16	>10000
13	38 ± 7	122.7 ± 21.7	343 ± 29	<5	75 ± 10	745 ± 303	43 ± 9	412 ± 266	nd	>10000
14	18629 ± 13202	1495.5 ± 99.5	>10000	10.5 ± 3.9	1049 ± 601	1960 ± 478	92 ± 4	2223 ± 64	3097 ± 430	>10000
15	353 ± 158.1	11 ± 2	466 ± 487	4.3 ± 2.2	308 ± 11	409 ± 122	399 ± 42	442 ± 118	413 ± 132	>10000
16	206 ± 13	12.8 ± 8.8	120 ± 86	7 ± 3	nd	nd	nd	nd	nd	nd
17	62.5 ± 1.6	<14	11 ± 5	26.9 ± 20	2 ± 1	21 ± 4	18 ± 1	nd	nd	>10000
25	nd	70.5 ± 11.5	3893 ± 275	20.7 ± 4.6	nd	nd	nd	nd	nd	nd
28	616.2 ± 415.7	1547 ± 101	311 ± 193	>9700	443 ± 173	797 ± 330	589 ± 199	nd	nd	>10000
31	41.6 ± 9	260 ± 18	49 ± 32	>9700	35 ± 1	101 ± 11	115 ± 3	nd	nd	>10000
32	nd	577 ± 282	213 ± 61	>9700	nd	nd	nd	nd	nd	nd
33	nd	37 ± 21	54	109.9 ± 41.1	71 ± 10	130 ± 11	222 ± 1	nd	nd	>10000
36	nd	55 ± 11	338 ± 21	321 ± 291	nd	nd	nd	nd	nd	nd
39	nd	121.3 ± 3.3	300	79 ± 13.3	nd	nd	nd	nd	nd	nd

EXPERIMENTAL SECTION

For full details, refer to the Supporting Information.

Virtual High Throughput Screening (VHTS). The virtual library was prepared by decoration of the tetrahydrobenzodiazepine (THB) core with 62 different R¹ and 62 different R² groups (62 × 62). The library was prepared in Pipeline Pilot. The structures were assembled, and stereoisomers and tautomers were enumerated. This database was minimized in MOE (version 2009.10) using database minimize, with MMFF94x force field and an rms gradient of 0.1. The crystal structures of RabGGTase, FTase, and GGTase I were prepared for docking by removal of the inhibitor and the prenylpyrophosphate, followed by the addition of hydrogens using the Protonate3D function in MOE. Ligands were docked into the proteins using GOLD (version 4.1.1). Since the imidazole is known to bind to the zinc atom, we set a binding constraint by defining an imidazole substructure with defined distance to the zinc atom (min 1.5 Å, max 3.5 Å, spring constant = 5). Further, the binding site was defined by a sphere of radius 15 Å around the phenylalanine/tyrosine residue. The Chemscore scoring function was used in combination with most accurate automatic genetic algorithm settings (autoscale = 1). Ten solutions were generated for all inhibitors. The scores for RabGGTase and FTase were compared for each inhibitor, assuming that an inhibitor with a high score for RabGGTase and a low score for FTase would be most selective. The compounds that satisfied these conditions and showed a preserved binding mode in RabGGTase were further evaluated for their synthetic feasibility and synthesized.

In Vitro Radioactive RabGGTase Assay. RabGGTase activity was measured employing the scintillation proximity assay (SPA),²⁴ and the experiment was performed in a 384-well plate format. A typical assay (20 μL scale) contained variable amounts of tested compounds in DMSO (0.4%), 4 nM RabGGTase, 0.5 μM geranylgeranyl pyrophosphate [³H], 1.5 μM geranylgeranyl pyrophosphate, 2 μM SUMO-HIS-Rab7, and 0.5 μM REP-1 in prenylation buffer (50 mM HEPES, pH 7.5, 50 mM NaCl, 2 mM MgCl₂, 0.5 mM TCEP, 20 μM GDP, 0.01% Triton X-100, 0.6% DMSO). Enzymatic reaction was conducted at room temperature for 1 h and was stopped by addition of 50 μL of stopper-bead mix (0.625 mg/mL copper chelate yttrium silicate SPA scintillation beads, 36% (w/v) ethanol, 50% (w/v) 2× PBS buffer with 0.4% BSA, 11% (w/v) H₂O). Beads were allowed to settle in the dark for 8 h. Plates were then measured employing a Wallac 1450 MicroBeta Trilux scintillation counter (Perkin-Elmer LAS GmbH). The readout of probes without inhibitor was defined as 100% activity, whereas the data of reactions without RabGGTase were defined as 0%. IC₅₀ determinations were calculated employing Quattro "Workflow" software (Quattro Research GmbH).

ASSOCIATED CONTENT

Supporting Information

Full experimental details, virtual screening procedures, crystal structure determination, and assay descriptions. This material is available free of charge via the Internet at <http://pubs.acs.org>.

AUTHOR INFORMATION

Corresponding Author

*For W.B.: (phone) (49) 921 55 2427; (e-mail) wulf.blankenfeldt@uni-bayreuth.de; (present address) Lehrstuhl für Biochemie, Universität Bayreuth, Universitätsstraße 30, 95447 Bayreuth, Germany. For R.S.G.: (phone) (49) 231 133 2300; (e-mail) goody@mpi-dortmund.mpg.de.

Author Contributions

[†]These authors contributed equally.

Notes

The authors declare no competing financial interest.

ACKNOWLEDGMENTS

We thank the X-ray communities of the Max-Planck-Institut für Molekulare Physiologie (Dortmund, Germany) and the Max-Planck-Institut für Medizinische Forschung (Heidelberg, Germany) for collecting diffraction data at the Swiss Light Source of the Paul Scherrer Institute (Villigen, Switzerland) and for giving us generous access to and support for station X10SA. The research leading to these results has received funding from the European Research Council under the European Union's Seventh Framework Programme (FP7/2007-2013)/ERC Grant Agreement No. 268309. This work was supported in part by DFG grants to H.W. and R.S.G. (Grant No. SFB642) and by the Zentrum für Angewandte Chemische Genomik. R.S.B. thanks the Alexander von Humboldt Stiftung for a fellowship. E.A.S. thanks the IMPRS-CB for a Ph.D. scholarship.

ABBREVIATIONS USED

DBU, 1,8-diazabicycloundec-7-ene; DCM, dichloromethane; DMAP, *N,N*-dimethylaminopyridine; DME, dimethoxyethane; DMF, *N,N*-dimethylformamide; FPP₂, farnesyl pyrophosphate; FTase, farnesyltransferase; GGPP, geranylgeranyl pyrophosphate; GGTase I, geranylgeranyltransferase; LBS, lipid binding site; NBD-FPP, 3,7,11-trimethyl-12-(7-nitrobenzo[1,2,5]-oxadiazol-4-ylamino)dodeca-2,6,10-trienyl pyrophosphate; RabGGTase₁, rab geranylgeranyltransferase; REP, rab escort protein; TAG, tunnel adjacent to GGPP binding site; Tf, trifluoromethylsulfonyl; TFA, trifluoroacetic acid; TFAA, trifluoroacetic anhydride; THB, tetrahydrobenzodiazepine; THF, tetrahydrofuran; VHTS, virtual high throughput screening

REFERENCES

- (1) Lane, K. T.; Beese, L. S. Structural biology of protein farnesyltransferase and geranylgeranyltransferase type I. *J. Lipid Res.* **2006**, *47*, 681–699.
- (2) Leung, K. F.; Baron, R.; Seabra, M. C. Thematic review series: lipid posttranslational modifications. Geranylgeranylation of Rab GTPases. *J. Lipid Res.* **2006**, *47*, 467–475.
- (3) Nguyen, U. T.; Goody, R. S.; Alexandrov, K. Understanding and exploiting protein prenyltransferases. *ChemBioChem* **2010**, *11*, 1194–1201.
- (4) Colicelli, J. Human RAS superfamily proteins and related GTPases. *Sci. STKE* **2004**, *2004*, RE13.
- (5) Schwartz, S. L.; Cao, C.; Pylpenko, O.; Rak, A.; Wandinger-Ness, A. Rab GTPases at a glance. *J. Cell Sci.* **2007**, *120*, 3905–3910.
- (6) Stenmark, H. Rab GTPases as coordinators of vesicle traffic. *Nat. Rev. Mol. Cell Biol.* **2009**, *10*, 513–525.
- (7) Reiss, Y.; Goldstein, J. L.; Seabra, M. C.; Casey, P. J.; Brown, M. S. Inhibition of purified p21ras farnesyl:protein transferase by Cys-AAX tetrapeptides. *Cell* **1990**, *62*, 81–88.
- (8) Seabra, M. C.; Reiss, Y.; Casey, P. J.; Brown, M. S.; Goldstein, J. L. Protein farnesyltransferase and geranylgeranyltransferase share a common alpha subunit. *Cell* **1991**, *65*, 429–434.
- (9) Appels, N. M.; Beijnen, J. H.; Schellens, J. H. Development of farnesyl transferase inhibitors: a review. *Oncologist* **2005**, *10*, 565–578.
- (10) Konstantinopoulos, P. A.; Karamouzis, M. V.; Papavassiliou, A. G. Post-translational modifications and regulation of the RAS superfamily of GTPases as anticancer targets. *Nat. Rev. Drug Discovery* **2007**, *6*, 541–555.
- (11) Sousa, S. F.; Fernandes, P. A.; Ramos, M. J. Farnesyltransferase inhibitors: a detailed chemical view on an elusive biological problem. *Curr. Med. Chem.* **2008**, *15*, 1478–1492.
- (12) Rose, W. C.; Lee, F. Y.; Fairchild, C. R.; Lynch, M.; Monticello, T.; Kramer, R. A.; Manne, V. Preclinical antitumor activity of BMS-214662, a highly apoptotic and novel farnesyltransferase inhibitor. *Cancer Res.* **2001**, *61*, 7507–7517.

- (13) Lackner, M. R.; Kindt, R. M.; Carroll, P. M.; Brown, K.; Cancilla, M. R.; Chen, C.; de, S. H.; Franke, Y.; Guan, B.; Heuer, T.; Hung, T.; Keegan, K.; Lee, J. M.; Manne, V.; O'Brien, C.; Parry, D.; Perez-Villar, J. J.; Reddy, R. K.; Xiao, H.; Zhan, H.; Cockett, M.; Plowman, G.; Fitzgerald, K.; Costa, M.; Ross-Macdonald, P. Chemical genetics identifies Rab geranylgeranyl transferase as an apoptotic target of farnesyl transferase inhibitors. *Cancer Cell* **2005**, *7*, 325–336.

- (14) Hutagalung, A. H.; Novick, P. J. Role of Rab GTPases in membrane traffic and cell physiology. *Physiol. Rev.* **2011**, *91*, 119–149.

- (15) Deraeve, C.; Guo, Z.; Bon, R. S.; Blankenfeldt, W.; Dilucrazia, R.; Wolf, A.; Menninger, S.; Stigter, E. A.; Wetzel, S.; Choidas, A.; Alexandrov, K.; Waldmann, H.; Goody, R. S.; Wu, Y. W. Psoromic acid is a selective and covalent Rab-prenylation inhibitor targeting autoinhibited RabGGTase. *J. Am. Chem. Soc.* **2012**, *134*, 7384–7391.

- (16) Guo, Z.; Wu, Y. W.; Tan, K. T.; Bon, R. S.; Guiu-Rozas, E.; Delon, C.; Nguyen, T. U.; Wetzel, S.; Arndt, S.; Goody, R. S.; Blankenfeldt, W.; Alexandrov, K.; Waldmann, H. Development of selective RabGGTase inhibitors and crystal structure of a RabGGTase-inhibitor complex. *Angew. Chem., Int. Ed.* **2008**, *47*, 3747–3750.

- (17) Tan, K. T.; Guiu-Rozas, E.; Bon, R. S.; Guo, Z.; Delon, C.; Wetzel, S.; Arndt, S.; Alexandrov, K.; Waldmann, H.; Goody, R. S.; Wu, Y. W.; Blankenfeldt, W. Design, synthesis, and characterization of peptide-based rab geranylgeranyl transferase inhibitors. *J. Med. Chem.* **2009**, *52*, 8025–8037.

- (18) Watanabe, M.; Fiji, H. D.; Guo, L.; Chan, L.; Kinderman, S. S.; Slamon, D. J.; Kwon, O.; Tamanoi, F. Inhibitors of protein geranylgeranyltransferase I and Rab geranylgeranyltransferase identified from a library of allenolate-derived compounds. *J. Biol. Chem.* **2008**, *283*, 9571–9579.

- (19) Baron, R. A.; Tavares, R.; Figueiredo, A. C.; Blazewska, K. M.; Kashemirov, B. A.; McKenna, C. E.; Ebetino, F. H.; Taylor, A.; Rogers, M. J.; Coxon, F. P.; Seabra, M. C. Phosphonocarboxylates inhibit the second geranylgeranyl addition by Rab geranylgeranyl transferase. *J. Biol. Chem.* **2009**, *284*, 6861–6868.

- (20) McKenna, C. E.; Kashemirov, B. A.; Blazewska, K. M.; Mallard-Favier, I.; Stewart, C. A.; Rojas, J.; Lundy, M. W.; Ebetino, F. H.; Baron, R. A.; Dunford, J. E.; Kirsten, M. L.; Seabra, M. C.; Bala, J. L.; Marma, M. S.; Rogers, M. J.; Coxon, F. P. Synthesis, chiral high performance liquid chromatographic resolution and enantiospecific activity of a potent new geranylgeranyl transferase inhibitor, 2-hydroxy-3-imidazo[1,2-*a*]pyridin-3-yl-2-phosphonopropionic acid. *J. Med. Chem.* **2010**, *53*, 3454–3464.

- (21) Bon, R. S.; Guo, Z.; Stigter, E. A.; Wetzel, S.; Menninger, S.; Wolf, A.; Choidas, A.; Alexandrov, K.; Blankenfeldt, W.; Goody, R. S.; Waldmann, H. Structure-guided development of selective RabGGTase inhibitors. *Angew. Chem., Int. Ed.* **2011**, *50*, 4957–4961.

- (22) Nguyen, U. T.; Guo, Z.; Delon, C.; Wu, Y.; Deraeve, C.; Franzel, B.; Bon, R. S.; Blankenfeldt, W.; Goody, R. S.; Waldmann, H.; Wolters, D.; Alexandrov, K. Analysis of the eukaryotic prenylation by isoprenoid affinity tagging. *Nat. Chem. Biol.* **2009**, *5*, 227–235.

- (23) Tong, H.; Holstein, S. A.; Hohl, R. J. Simultaneous determination of farnesyl and geranylgeranyl pyrophosphate levels in cultured cells. *Anal. Biochem.* **2005**, *336*, 51–59.

- (24) Glickman, J. F.; Schmid, A.; Ferrand, S. Scintillation proximity assays in high-throughput screening. *Assay Drug Dev. Technol.* **2008**, *6*, 433–455.